This is a preprint, the final version is subject to change, of the American Mineralogist (MSA)
Cite as Authors (Year) Title. American Mineralogist, in press.
(DOI will not work until issue is live.) DOI: http://dx.doi.org/10.2138/am.2014.4636

REVISION 2

Effect of oxalate and pH on chrysotile dissolution at 25ºC: An experimental study

Marisa Rozalen,*[,1] M. Elena Ramos,[1] Saverio Fiore,[2] Fernando Gervilla,[1,3]
and F. Javier Huertas[1]

[1]Instituto Andaluz de Ciencias de la Tierra (CSIC-University of Granada),
Avda. de las Palmeras 4, 18100 Armilla, Granada, Spain

[2]Institute of Methodologies for Environmental Analysis, CNR, Tito Scalo, Potenza, Italy

[3]Departamento de Mineralogía y Petrología, Universidad de Granada,
Avda. Fuentenueva s/n, 18071 Granada, Spain

Manuscript submitted to:

American Mineralogist

* Corresponding author:
Marisa Rozalen
Telephone: +34 958 230000 ext. 190120
E-mail: marisarozalen@ugr.es: mlrozalen@gmail.com

This is a preprint, the final version is subject to change, of the American Mineralogist (MSA)
Cite as Authors (Year) Title. American Mineralogist, in press.
(DOI will not work until issue is live.) DOI: http://dx.doi.org/10.2138/am.2014.4636

ABSTRACT

The effect of pH on the kinetics of chrysotile dissolution was investigated at 25 °C in batch reactors over the pH range of 1 to 13.5, in oxalic solutions and buffered solutions of inorganic salts. Dissolution rates were obtained based on the release of Si and Mg. Results of the batch with inorganic buffers showed a strong dependence of dissolution rates on pH in the acid range. The logarithm of dissolution rates decreases with the pH with a slope of $n = 0.27$. Around neutral pH, a minimum is reached. From pH 8 to 12, rates increase again when pH increases, and follow a linear dependence with a shallow slope ($n = 0.06$). The Mg/Si ratio shows a non-stoichiometric dissolution reaction with a preferential release of Mg^{2+} at acidic pH; it decreases at neutral pH conditions according to Mg solubility. Our results suggest that the relative ease of the breaking of Mg–O bonds compared with Si–O bonds lead to dissolution via a series of steps involving Si and Mg, where Si release is the rate-limiting step.

In the presence of 15 mmol L^{-1} oxalate, an intense catalytic effect from pH 1 to 6 is observed because of the capacity of the oxalate anion to form different complexes with Mg. The ratio of the rates derived from Mg and Si concentrations confirm an enhancement of non-stoichiometric dissolution compared with the series without oxalate. The mechanism of catalysis involves different processes depending on pH: At pH 1, XRD analysis confirms the formation of an amorphous silica phase dissolving all the Mg present in the chrysotile structure. At pH 2, XRD and FTIR results also confirm the precipitation of glushinskite, a magnesium oxalate phase. At pH 3 to 6, the presence of oxalate enhances dissolution almost by an order of magnitude compared with the experiments in inorganic buffered solutions. In this case, the mechanism could be due to the formation of aqueous or surface magnesium oxalate complexes.

This is a preprint, the final version is subject to change, of the American Mineralogist (MSA)
Cite as Authors (Year) Title. American Mineralogist, in press.
(DOI will not work until issue is live.) DOI: http://dx.doi.org/10.2138/am.2014.4636

However, dissolution rates at neutral pH in the presence of oxalate are similar to those obtained in inorganic buffered solutions; the pH dependence at pH 8 to 13 is minimal. The increase in saturation and the drastic decrease in Mg solubility at these pH values could lead to precipitation of secondary phases coating the reactive mineral surface and inhibiting the surface.

Results obtained in this study show that chrysotile dissolves faster in acid media and oxalate acts a strong catalyst increasing the efficiency of magnesium release to solution at ambient temperature. These data may provide an excellent background to design and select optimal conditions in the previous acid treatment for carbon capture processes, as well as help to develop remediation process of asbestos contaminated sites.

Keywords: Chrysotile, asbestos, dissolution, oxalate

This is a preprint, the final version is subject to change, of the American Mineralogist (MSA)
Cite as Authors (Year) Title. American Mineralogist, in press.
(DOI will not work until issue is live.) DOI: http://dx.doi.org/10.2138/am.2014.4636

INTRODUCTION

Chrysotile, together with some members of the amphiboles, when they occur in an asbestiform habit, are regulated as asbestos (Gunter et al., 2007a). This is an industrial term that describes several silicate minerals which form long, thin, durable mineral fibers with high tensile strength, flexibility, and heat resistance (Skinner et al. 1988; Virta 2005; Van Gosen 2007). Because of these properties, they were widely used as building insulators, fire and heat protection materials, pipeline wrapping, and so forth, before they were linked to several pulmonary health problems including asbestosis, lung cancer, and mesothelioma (Skinner et al. 1988; ATSDR 2001; Roggli and Coin 2004). Even though at present they are banned in 52 countries, the so-called "controlled use" of chrysotile asbestos is often exempted from the ban. In fact, chrysotile accounts for more than 95% of the asbestos used globally (LaDou et al. 2010).

Chrysotile abundance, usefulness, and hazardous properties have lead to early interest in fields as geochemistry, medicine, and biology. Geochemical studies have focused on the dissolution kinetics (Wood et al. 2006; Taunton et al. 2010), calculation of the biodurability of the fibers in simulated lung fluids (Taunton et al. 2010; Oze and Solt 2010), and acid treatments for developing environmental remediation processes. The mechanism of chrysotile dissolution is also of critical importance for engineered carbon capture. (e.g. O'Connor et al., 2002; Park et al., 2003; Park and Fan, 2004).

Hargreaves and Taylor (1946) reported that magnesium could be completely removed from the chrysotile structure by treatment with dilute acid. Later, many other studies have focused on acid leaching (e.g., Nagy and Bates 1952; Thomassin et al. 1977; Allen and Smith 1994; Rozalen and Huertas 2013). More recently, Wypych et al. (2005) found that the leached byproducts consist of layered hydrated disordered silica with a distorted structure resembling the tetrahedral silica layer in the original mineral. Studies of dissolution at basic pH are also

This is a preprint, the final version is subject to change, of the American Mineralogist (MSA)
Cite as Authors (Year) Title. American Mineralogist, in press.
(DOI will not work until issue is live.) DOI: http://dx.doi.org/10.2138/am.2014.4636

scarce because of the difficulty associated with the low solubility of Mg in basic solutions and its ease of saturation with respect to brucite and magnesite (e.g., Luce et al. 1972; Lin and Clemency 1981). Choi and Smith (1972) studied dissolution at 5–45 °C and pH 6–10, and obtained activation enthalpies between 5.5–6.5 kcal mol^{-1}. They suggested that the rate-controlling mechanism was diffusion of Mg and OH^- ion from the surface into solution. Later on, Bales and Morgan (1985) measured dissolution rates derived from Mg release in short-time batch experiments (5 days), and obtained a fractional pH dependence ($[H]^{0.24}$) at pH 7 to 10. Dissolution rates derived from Si release did not show definite pH dependence. In other words, dissolution data for chrysotile are scarce and sometimes controversial because of differences in experimental procedures. Because of the growing interest in geochemical data in the fields of medical geology or environmental remediation, it is a clear necessity to obtain the profile of dissolution rate dependence on pH in order to evaluate the effect of weathering of these minerals at the laboratory scale. These data can be useful not only in the range of natural waters but also under very acidic conditions (e.g., effect of acid rain or mine drainage waters on naturally occurring minerals) or very basic ones (e.g., magnesium silicate dissolution rates together with precipitation rates of magnesium carbonates allow the quantitative modeling and assessment of various CO_2 scenarios e.g., Bergman and Winter 1995).

On the other hand, the role of soil organic acids in enhancing chemical weathering rates has been recognized for decades. Many studies show that polyfunctional acids such as oxalic acid and citric acid enhance silicate dissolution more than do monofunctional acids such as acetic acid (Huang and Kiang 1972; Franklin et al. 1994; Wang et al. 2005; Ramos et al. 2011). Although several studies have quantified the oxalate effect in many minerals like olivine (Liu et al. 2006; Olsen and Rimstidt 2008; Prigiobbe and Mazzotti 2011) and kaolinite (Cama and Ganor 2006) none of them have quantified this effect in chrysotile. Moreover,

This is a preprint, the final version is subject to change, of the American Mineralogist (MSA)
Cite as Authors (Year) Title. American Mineralogist, in press.
(DOI will not work until issue is live.) DOI: http://dx.doi.org/10.2138/am.2014.4636

studies on chrysotile have not focused on the alteration mechanism or obtain dissolution rates. The principal aim is the destruction of the fibers using different techniques, including treatments with oxalic acid. Favero-Longo et al. (2005) studied the degradation of Italian chrysotile through field and laboratory studies. Collecting samples in the natural outcrop, they observed that lichens secrete oxalic acid, and degrade the fibers into an amorphous material by a long-term natural process. Other studies, such as those of Turci et al. (2008, 2010), used oxalic acid treatments after ultrasonication of samples in order to increase the mineral surface area and increase the efficiency of the fibers destruction process.

Some authors like Wood et al. (2006) did model dissolution at both pH 4 and 7.34 to simulate the conditions in a lung macrophage and lung fluid, respectively. However, these correspond to specific pH conditions and solution compositions. Despite its importance, there is a lack of experimental data that quantify the relation between dissolution and pH. It is well known that oxalate is able to destroy chrysotile fibers at very acidic pH, although the mechanism of transformation and the effect of this ligand at other pH values are still unknown. The objectives of this study were i) to evaluate the effect of pH at earth surface conditions (pH 1–13), ii) to obtain insights into the dissolution mechanism, and iii) to quantify the catalytic effect of oxalate in dissolution at various pH values.

MATERIALS AND METHODS

Characterization of the mineral sample

All experiments were carried out on chrysotile collected from Mina Laurel, an old asbestos mine in Ojén Ultramafic Massif (Málaga, Spain). Chrysotile fibers fill a network of 1–2 cm thick fractures that cut the partially altered peridotite host rock, and grow approximately perpendicular to the fracture walls (Fig. 1). The mineral was separated from

the host rock using a saw. Afterward, the chrysotile was milled, suspended in water using a mechanical stirrer, and allowed to settle for two hours. The 10 cm supernatant was siphoned, centrifuged, recovered with acetone, dried in an oven at 40 °C, and then stored in a polyethylene bottle. Several sedimentation–suspension cycles were performed on the milled material. The sedimentation conditions correspond to □4 μm equivalent diameter. Although Stoke's law cannot be properly applied to fibrous material, this procedure allowed us to minimize the amount of minerals accompanying chrysotile.

The resulting material was studied by X-ray diffraction (XRD) using a PANalytical X'Pert Pro diffractometer with a X'Celerator detector. The diffraction pattern corresponds to pure chrysotile. The images obtained by scanning electron microscopy (SEM; LEO 1430-VP), show a material composed of fiber bundles, from tens to hundreds of micrometers in length, with a wide variety of length-to-diameter ratios (Fig. 2). The composition of individual fibers was obtained by transmission and analytical electron microscopy (TEM–AEM; Philips CM20). The average composition obtained from several tens of fiber analyses has the following chrysotile structural formula:

$$Ca_{0.02}Mg_{2.75}Fe_{0.10}Al_{0.06}Si_2O_5(OH)_4$$

The corresponding Mg/Si atomic ratio is 1.38.

The specific surface area of the chrysotile was measured by the Brunauer-Emmett-Teller (BET) method, using 5-point N_2 adsorption isotherms, after degassing the sample for 60 min at 120°C. The specific surface area was 36.8 m^2g^{-1} (with an estimated uncertainty of 10%).

Experimental design

Short-term (30 days) dissolution experiments were carried out in batch reactors at a solid/solution ratio of 2 g L^{-1}. The mineral sample was placed directly in acid-cleaned PFA

This is a preprint, the final version is subject to change, of the American Mineralogist (MSA)
Cite as Authors (Year) Title. American Mineralogist, in press.
(DOI will not work until issue is live.) DOI: http://dx.doi.org/10.2138/am.2014.4636

bottles containing 250 mL of buffered solutions at pH 1 to 13.5 (Table 1). To prevent oversaturation of solutions, experiments at very basic pH (11–13) were repeated using a solid/solution ratio of 0.1 g L^{-1} for 15 days. Two sets of experiments were performed using inorganic buffered solutions (series CrLx) and the same solutions with 15 mmol L^{-1} sodium oxalate (series CrOx). The temperature was controlled by partially immersing the reaction vessels in a water bath at thermostated at 25 ± 2 °C. The spongy and fibrous morphology of this chrysotile sample tends to clog the tip of the pipettes in many cases and did not allow taking aliquots keeping the ratio A/V constant. Consequently we let the solid settle down, aliquots of solution were withdrawn periodically, and then filtered through a 0.22 μm Durapore membrane into an acid-cleaned polyethylene bottle.

The solution pH was measured at room temperature immediately after filtration using a Crison combination electrode standardized with pH 4.01 and 7.00 buffer solutions. The reported accuracy was ±0.02 pH units. The solutions were acidified with ultrapure HNO_3 to pH 3 if necessary to prevent precipitation during storage for Si and Mg analysis. The silicon concentration in every withdrawal was determined by colorimetry using the molybdate blue method (Grasshoff et al. 1983) with a detection limit of 5 ppb and an associated error of 5%. The magnesium concentration in every withdrawal was determined by ion chromatography (IC; Metrohm 883 Basic IC Plus Ion Chromatograph) using a Metrosep C3-250 column. The eluent was prepared with 3.5 mmol L^{-1} HNO_3. The detection limit and associated error were 1 ppb and 3%, respectively. Dissolved aluminum was measured by fluorimetry using lumogallion as complexing agent (Hydes and Liss 1976). The method had a detection limit of 0.3 ppb and an associated error of 3%. To control possible degradation, the oxalate concentration in some selected withdrawals was measured by IC, using with a Metrosep A Supp 4-250 column with chemical suppression, as well as 1.7 mmol L^{-1} $NaHCO_3$ and 1.8 mmol L^{-1} $NaCO_3$ solution as eluent. The detection limit was 0.9 ppm and the associated error

This is a preprint, the final version is subject to change, of the American Mineralogist (MSA)
Cite as Authors (Year) Title. American Mineralogist, in press.
(DOI will not work until issue is live.) DOI: http://dx.doi.org/10.2138/am.2014.4636

was 5%. Once the experiments were completed, the remaining solids were rinsed with Milli-Q water, dried in acetone, and then stored for further XRD, Fourier transform infrared spectroscopy (FTIR) and SEM analyses.

Dissolution rate calculations

In the batch experiments, the dissolution rate was computed from the variation of component *j* concentration in the reactive solutions as time progresses (Rozalen et al. 2008):

$$Rate_j = \frac{1}{\upsilon_j}\frac{V}{SM}\frac{dC_j}{dt} \quad (1)$$

where ν_j is the stoichiometric coefficient of component *j* in the dissolution reaction, *M* represents the mass of chrysotile (g), S is the BET surface area ($m^2 \cdot g^{-1}$), *V* is the volume of solution (L), C_j is the concentration of component *j*, and *t* represents time (s). The uncertainty associated with the rate constants around 15% and was dominated by the uncertainty in concentration measurements, BET area and slope calculation. All rates were normalized to surface area (mol $m^{-2}s^{-1}$) by convention using the Si concentration, and Mg was used to evaluate stoichiometry of the reaction. The discussion about the reactive surface area of silicates is still under debate, far from the scope of this study. BET surface area not always represents the reactive surface area of a phyllosilicate (e.g., Metz et al. 2005; Rozalen et al. 2008), and rates normalized to initial mass (mol $g^{-1}s^{-1}$) may be more reliable. Conversion to different rate units is simple if the surface are is provided. .

Periodic sampling of the batch experiments introduces a change in the solid/solution ratio. Therefore, the Mg and Si concentrations were corrected to standardize the analyses for the initial solid/solution ratio and actual volume by applying the correction factor used by Olsen and Rimstidt (2008):

This is a preprint, the final version is subject to change, of the American Mineralogist (MSA)
Cite as Authors (Year) Title. American Mineralogist, in press.
(DOI will not work until issue is live.) DOI: http://dx.doi.org/10.2138/am.2014.4636

$$C_{j,ideal} = \frac{1}{V_0}\sum_{i=1}^{n}\Delta c_i V_{i-1} \quad (2)$$

where $C_{j,ideal}$ is the standardized concentration of species j, V_0 is the initial volume, c_i is the concentration of component j at withdrawal i, V_{i-1} is the remaining volume at withdrawal $i-1$, and the sum is extended from 1 to $i = 1, 2, \ldots n$.

Saturation calculations

Chrysotile ideally dissolves according to the following hydrolysis reaction:

$$Ca_{0.02}Mg_{2.75}Fe_{0.10}Al_{0.06}Si_2O_5(OH)_4 + 6H \longrightarrow$$

$$\longrightarrow 0.02Ca^{2+} + 2.75Mg^{2+} + 0.10Fe^{3+} + 0.06Al^{3+} + 2SiO_2 + 5\,H_2O$$

The equilibrium constant for this reaction was estimated according to Vieillard et al. (2000), and a value of $\log K_{eq} = 25.29$ was obtained.

The saturation state of the solution with respect to the solid phases was calculated in terms of the free energy of reaction ΔG_r:

$$\Delta G_r = -RT\ln\left(\frac{IAP}{K_{eq}}\right) \quad (3)$$

where R is the gas constant, T is the absolute temperature, and IAP and K_{eq} respectively represent the ion activity product and the equilibrium constant for the dissolution reaction. Aqueous activities and chemical affinities in the present study were generated using the EQ3NR geochemical code (Wolery, 1992). The IAP was calculated from the pH, as well as the concentrations of Si, Mg, and Al measured in every batch experiment. Mg was introduced in equilibrium with brucite above pH 11. The iron concentration was below detection limit. The iron introduced in the EQ3NR input files was stoichiometric with Si at acidic conditions,

This is a preprint, the final version is subject to change, of the American Mineralogist (MSA)
Cite as Authors (Year) Title. American Mineralogist, in press.
(DOI will not work until issue is live.) DOI: http://dx.doi.org/10.2138/am.2014.4636

or in equilibrium with Fe hydroxides in solutions above pH 4. Furthermore, the code was used to model the capacity of oxalate to form aqueous Mg species. The aqueous magnesium oxalate complexes were implemented in the Lawrence Livermore National Laboratory thermodynamic database (data0.cmp in EQ3/6 package) using reactions of aqueous Mg^{2+} and $C_2O_4^{2-}$ at 25 °C (Table 2) (Wolery 1992; Sillen and Martell 1964).

RESULTS

Series without oxalate (CrLx)

The evolution of pH, as well as the Si and Mg concentrations in the batch experiments for some representative examples are illustrated in Figure 3. The pH of the solutions remains stable during most of the experiments. However, at slightly acidic or near neutral conditions (pH 4, 5, and 6), the pH drifted from the initial value and stabilized later at pH 7–8 probably because of the strong consumption of protons during the dissolution reaction. In general, Si is rapidly released (after one or two days), although concentrations are linearly proportional to the elapsed time until 20–30 days in most of the experiments. The Si release rate increases linearly with elapsed time at very basic conditions only (pH > 11), but tends to stabilize as the solution becomes more saturated. Dissolution rates for constant pH conditions were computed using the Si concentrations in the interval of linear release proportional to elapsed time between 11 to 20 days, after the initial rapid dissolution stage (dissolution of surface defects and small particles) and before saturation is reached. As it is discussed in Rozalen et al. (2008) the zone where Si concentration slope is measured in batch reactors to obtain dissolution rates is tricky. In order to get rates equivalent to steady state ones (as it occurs in flow-through experiments) the amount of silica liberated to the solution in every withdrawal

This is a preprint, the final version is subject to change, of the American Mineralogist (MSA)
Cite as Authors (Year) Title. American Mineralogist, in press.
(DOI will not work until issue is live.) DOI: http://dx.doi.org/10.2138/am.2014.4636

of the batch reactor should be the constant and far from equilibrium conditions should be attained.

The release of Mg is similar to that of Si at pH 1 to 4, but shows a preferential release of Mg versus Si (Figs. 3d and 3e). At pH 5 to 9, the Mg concentration is lower than that of Si (e.g., Fig. 3f). At pH 10 to 13, the Mg concentration is below the detection limit. Dissolution rates were computed for constant-pH conditions using the Mg concentrations in the same interval as silica rates in order to evaluate stoichiometry of the reaction (Table 3). All concentration vs time experimental measurements are available as supplementary data in an electronic file.

Series with oxalate (CrOx)

The evolution of pH, Si, and Mg concentrations in batch experiments shows that oxalate has a strong catalytic effect on the element release into solution. This necessitates explaining the results at almost every pH. Figure 4 illustrates some representative examples.

At pH 1, the pH remains stable. The Si and Mg concentrations increase linearly with the elapsed time and tend to stabilize at 15 days (Fig. 4a). The Mg/Si measured ratio shows a preferential release of Mg concentrations around 10 times higher than that of Si (Fig. 4b). Moreover, the measured concentration of oxalate shows a progressive decrease from 15 to 12 mmol L^{-1}.

At pH 2, the presence of oxalate during the alteration causes a severe drift of pH from 2 to 6, and a preferential release of Mg versus Si (Fig. 4c). At the beginning of the experiment, the Mg/Si ratio reaches values higher than 12, and decreases asymptotically until 3(Fig. 4d). This effect is linked to a progressive decrease in the measured oxalate concentration from 15 to 7 mmol L^{-1}.

Experiments at initial pH values of 3 to 6 show drifts from the initial value and then a tendency to stabilize around pH 7, which is probably due to the strong consumption of protons during the dissolution reaction. As a general trend, Si and Mg are rapidly released although concentrations become linearly proportional to the elapsed time until 15 days. The Mg/Si measured ratio shows a preferential release of Mg at pH 3 and 4, which decreases progressively until the Mg/Si ratio is equal to 1 at pH 5 and 6. The measured concentration of oxalate does not show degradation of the ligand.

At pH 7, the solution pH drifts until pH 8. Release of silica and magnesium follows the general trend but the measured Mg/Si ratio is around 0.8, which corresponds to the low solubility of magnesium in basic media.

Experiments performed at initial pH values of 8 and 9 shows a stable pH with respect to time. Si and Mg concentrations increase with time. Again, the Si release is now higher than that of magnesium, as shown in Figure 4g. Finally, experiments from pH 10 to 13 show a stable pH with elapsed time. Si concentrations increase linearly as time progresses and tend to stabilize as the solution becomes saturated. No Mg data are available because it is below detection limit. All concentration vs. time experimental measurements are available as supplementary data in an electronic file.

The instability of any of the rate-controlling parameters does not allow us to derive dissolution rates at steady-state conditions, as it occurs for CrLx series. For the CrOx experimental series, the pH drift occurs from acid to neutral pH. However, this pH drift is a consequence of the intense catalytic effect of oxalate, which is clear in all experiments with initial pH of 1 to 7. Figure 5 illustrates a representative experiment at pH 4 with and without oxalate. The amount of Si and Mg dissolved is up to 6–7 times higher in the presence of oxalate at pH 4 than without oxalate. In order to compare results with and without oxalate, other investigators have used the initial-rate method (Olsen and Rimstidt 2008). This method

This is a preprint, the final version is subject to change, of the American Mineralogist (MSA)
Cite as Authors (Year) Title. American Mineralogist, in press.
(DOI will not work until issue is live.) DOI: http://dx.doi.org/10.2138/am.2014.4636

303 determines the rate at the beginning of the experiment before any of the rate-controlling
304 parameters has changed from the original values (Laidler 1987; Rimstidt and Newcomb
305 1993). Nevertheless, it is necessary to remark that this is just a mathematical tool. Dissolution
306 rates obtained are labeled as "initial rates" because they are not measured at steady-state
307 conditions and do not represent the mineral dissolution rate at steady state. Initial dissolution
308 rates are faster and not straightforwardly comparable with the steady-state dissolution rates
309 obtained in the previous subsection.

310

311 **DISCUSSION**

312 **Dissolution rates and mechanism without oxalate**

313 The ratio of dissolution rates derived from Mg and Si concentrations shows non-
314 stoichiometric dissolution with a preferential release of Mg^2 at acidic pH; it decreases at
315 neutral pH conditions according to Mg solubility (Table 3). Incongruent dissolution generally
316 occurs in magnesium silicate minerals under neutral or alkaline conditions, and it is related to
317 magnesium solubility. Moreover, a preferential release of Mg over Si at steady state has been
318 observed in many acid dissolution studies on phyllosilicates, and has been attributed to rapid
319 ion-exchange reactions between the solution and the outermost part of the octahedral sheet
320 (e.g., Kohler et al. 2005; Bibi et al. 2011).

321 EQ3NR calculations showed values of $\Delta G_r < 0$ in all experiments at pH 1 to 8 (Table 3).
322 Note that ΔG_r values were calculated for every withdrawal in the experiments, but only the
323 highest and lowest values are given in the table to avoid data overloading (the complete
324 dataset is available at the supplementary online file). These results also show undersaturation
325 with respect to other minerals like brucite, magnesite, amorphous silica, and crystalline silica
326 polymorphs (Table 4). Unfortunately, we did not find in literature any ΔG_r value to delimit far

This is a preprint, the final version is subject to change, of the American Mineralogist (MSA)
Cite as Authors (Year) Title. American Mineralogist, in press.
(DOI will not work until issue is live.) DOI: http://dx.doi.org/10.2138/am.2014.4636

ad close to equilibrium conditions for chrysotile dissolution.The proximity to equilibrium is experimentally unavoidable under near-neutral conditions. Moreover, Mg solubility drastically decreases at pH > 9. As EQ3NR calculations show, supersaturation with respect to chrysotile and other Mg secondary phases is reached (Table 4). New phases were not detected by XRD, FTIR, or SEM investigations.

In order to ascertain if dissolution rates are affected by saturation, batch experiments at pH 10–13 were repeated using a solid/solution ratio 20 times smaller, that is, 0.1 g L^{-1} for 15 days (series CrLx_15d). These conditions represent an experimental compromise because the decrease in the solid/solution ratio leads to cation concentrations close or below detection limit, which would increase the uncertainty associated with the calculated rate. Even though the solid/solution ratio was lowered 20 times, the EQ3NR calculations showed that only experiments at pH 10 take place under subsaturation conditions (see Tables 3 and 4). At pH 11 to 13, the ΔG_r values are lower than in series CrLx, but still indicate oversaturation. Consequently, it is not possible to obtain values corresponding to far-from-equilibrium conditions in this pH range by using batch experiments. This fact is consistent with data reported in literature, which show that many near-neutral solutions used in dissolution experiments are supersaturated with respect to one or more secondary phases (e.g., Bales and Morgan (1985) for chrysotile or Taunton et al. (2010) for brucite in simulated lung fluids).

Finally, the dissolution rates derived from both series of experiments (Table 3) differ in half order of magnitude. Nevertheless, the slope in the basic branch remains constant and the reaction order is similar in both series. This indicates that saturation may affect the net dissolution rate, but the mechanism remains unaltered. Dissolution rates calculated from Si and Mg concentrations are shown in Table 3. As seen in Figure 6, the effect of pH on the chrysotile dissolution rate strongly depends on pH. At acidic pH (1–7), the logarithm of dissolution rates, which are calculated from the Si concentration, decreases when the pH

This is a preprint, the final version is subject to change, of the American Mineralogist (MSA)
Cite as Authors (Year) Title. American Mineralogist, in press.
(DOI will not work until issue is live.) DOI: http://dx.doi.org/10.2138/am.2014.4636

increases. A simple linear regression of the logarithm of rate versus pH produces the equation:

$$\log R_{Si}(mol/m^2s) = -0.27(\pm 0.02)\cdot pH - 10.87(\pm 0.08) \quad (4)$$

Equation 4 can be transformed to the rate law:

$$R_{Si}(mol/m^2s) = 10^{-10.87(\pm 0.08)}\cdot a_{H+}^{0.27(\pm 0.02)} \quad (5)$$

A minimum is reached at around pH 8–8.5, which is consistent with data obtained by Bales and Morgan (1985). At pH 8 to 12, rates again increase when the pH increases, following a linear dependence but with a smoother slope, n= 0.06. The corresponding lineal regression and derivative rate law are:

$$\log R_{Si}(mol/m^2s) = 0.06(\pm 0.01)\cdot pH - 13.37(\pm 0.06) \quad (6)$$

$$R_{Si}(mol/m^2s) = 10^{-13.37(\pm 0.06)}\cdot a_{H+}^{0.06(\pm 0.01)} \quad (7)$$

Statistical analysis of variance (ANOVA) for lineal regressions (4) and (6) show values of regression coefficients (R^2>0.9) and highly significant (P<0.001), thus indicating that the variation with pH at acid and basic pHs is significant.

At pH 12 and above, a slight decrease in rates was observed probably because of carbonation of Mg in our open-air experiments, as documented by Halder and Walther (2011) for enstatite dissolution. They suggested the inhibition of dissolution rates above pH 10 when experiments are open to the atmosphere. The carbonate dissolved in these solutions becomes dominantly CO_3^{2-} above pH 10 and forms a >Mg_2–CO_3 surface complex at the positively charged Mg surface sites on enstatite, resulting in stabilization of the surface Si–O bonds. On the other hand, Mg can also precipitate as microcrystalline brucite, as described for alkaline dissolution of other silicates (e.g., Fernandez et al. 2006).

This is a preprint, the final version is subject to change, of the American Mineralogist (MSA)
Cite as Authors (Year) Title. American Mineralogist, in press.
(DOI will not work until issue is live.) DOI: http://dx.doi.org/10.2138/am.2014.4636

As generally accepted for 2:1 phyllosilicates, the octahedral cations are released to the solution more readily than are tetrahedral cations (e.g., Brantley and Chen 1995; Lasaga 1995; Nagy 1995; Hume and Rimstidt 1992; Zysset and Schindler 1996; Jurinski and Rimstidt 2001; Kalinowski and Schweda 2007; Rozalen et al. 2008; Bibi et al. 2011). Therefore, for chrysotile, the relative ease of breaking of Mg–O bonds compared with Si–O leads to dissolution via a series of steps involving Si and Mg, Si being released in the rate-limiting step. This is supported by our experimental results at pH 1 to 8, where measured rates from silica concentrations are lower than rates measured from Mg data: $R_{Si} < R_{Mg}$ (Table 3).

Consequently, in acidic media, dissolution rates strongly depend on the pH. The number of protons required to break these metal–oxygen bonds depends on the valence of the metal atom (Oelkers and Schott 2001). Magnesium has a valence smaller than that of silica, and fewer protons are necessary to attack the metal–oxygen bonds; hence, Mg ions are released from the surface faster than Si. Finally, the metal–proton exchange reactions lead to Si-rich surfaces of multioxide minerals at acidic pH, which enhances release of lower-valence cations. The reverse phenomenon occurs at alkaline pH (Oelkers et al. 2009). This conclusion is consistent with the Pauling bond strength of the involved bonds, that for Si-O bond is 1 and for Mg^{VI}-O is 0.33. The Mg loss is extreme at pH 1, as confirmed by our XRD results after dissolution experiments (Fig. 7). The loss of intensity and height of the characteristic reflections of chrysotile after reaction points out the degradation of the initial mineral to a siliceous material with low crystallinity (broad band centered at 3.8 Å after 30 days at pH 1) (Fig. 7b). Microanalysis results obtained by using SEM (Fig. 8) indicate that some of the Mg is still in the chrysotile structure. This confirms a high resistance of Si–O bonds even when almost all of the Mg is out of the structure the morphology of the fibers is preserved, as SEM images confirm. Above pH 2, Mg is preferentially released but no changes are observed in the XRD pattern.

This is a preprint, the final version is subject to change, of the American Mineralogist (MSA)
Cite as Authors (Year) Title. American Mineralogist, in press.
(DOI will not work until issue is live.) DOI: http://dx.doi.org/10.2138/am.2014.4636

In basic media, dissolution rates are affected by the attack of hydroxyls to the Mg–O and Si–O bonds (e.g., Lasaga, 1995), the increase in saturation, and the drastic decrease in Mg solubility at these pH values. The latter factors could lead to precipitation of secondary phases (like brucite or magnesium carbonates above pH 12) that coat the reactive mineral surface and inhibit the attack of hydroxyls. The combination of these processes causes an apparent slight dependence of the dissolution rate on the pH in the basic branch. Furthermore, chrystalline or amorphous Mg phases in trace amount were detected by either XRD or SEM.

Dissolution and mechanism in presence of oxalate

Initial rates were calculated for oxalate experiments using the slopes from the first six days of reaction. They were also recalculated for oxalate–free experiments using the same time interval. The uncertainty associated is lower than 15%. A correction for sample withdrawal was applied in every case. The results of initial rates and ΔG_r recalculated with EQ3NR for this first 6–10 days are shown in Table 5 and illustrated in Figure 9. As observed in Table 5, the calculated ΔG_r values are similar for series CrLx and CrOx (without and with oxalate), showing undersaturation (far from equilibrium) conditions for experiments at pH 1 to 5. Around neutral pH, saturation values increase, and from pH 9 and above, solutions are supersaturated. Moreover, the saturation state calculated for different mineral phases are shown in Table 6. As explained in the previous subsection, this situation is experimentally unavoidable.

Nevertheless, the initial-rate results quantify the strong catalytic effect of oxalate at pH 1 to 6 despite the experimental limitations. This effect is stronger between pH 3.6 and 5.4, and increases by up to 0.8 logarithmic unit with respect to the oxalate-free dissolution rate at the same pH. This pH range corresponds to the maximum formation of the magnesium oxalate aqueous complex (Fig. 9b).

This is a preprint, the final version is subject to change, of the American Mineralogist (MSA)
Cite as Authors (Year) Title. American Mineralogist, in press.
(DOI will not work until issue is live.) DOI: http://dx.doi.org/10.2138/am.2014.4636

Based on these results and solid analysis, different mechanisms can contribute to the enhancement of chrysotile dissolution rates in oxalate solutions. Moreover, different processes take place at every pH, as solid sample analysis point out:

At pH 1, Si release to the solution is similar with and without oxalate. However, Mg release is significantly higher in the presence of this ligand. The XRD patterns (Fig. 7c) confirm the transformation of the initial chrysotile into amorphous silica byproduct. These results are similar to those obtained by Wang et al. (2006) and Gunter et al. (2007b). Moreover, SEM observations clearly show that the fiber morphology is preserved, but the EDS result suggests the complete removal of the brucite sheet from the chrysotile structure in the presence of oxalate. Also, the XRD patterns show no other accompanying phases, such as talc or amphiboles, that would have remained after chrysotile dissolution, as shown in Gunter et al. (2007b).

At pH 2, the presence of oxalate during the alteration causes an intense drift on pH from 2 to 6 and a preferential release of Mg versus Si (Mg/Si concentration ratio increases up to 3 times). These facts, together with a decrease in oxalate concentration (from 15 to 7 mmol L^{-1}), suggest that oxalate and aqueous Mg can precipitate and shift the overall reaction to the right:

$$Mg_3Si_2O_5(OH)_4\ \ 6H + 3C_2O_4^{2-} \rightarrow 3MgC_2O_4\ \ 2SiO_2\ \ 5H_2O \qquad (8)$$

XRD results (Fig. 10a) confirm the formation of a precipitate identified as glushinskite, a magnesium oxalate hydrate. FTIR spectra also show noticeable changes after dissolution (Fig. 10b). In the reacted sample, new spectrum bands appear with respect to the initial sample spectrum, which confirm the formation of a new magnesium oxalate solid phase, as described in Table 7 and Figure 10b. Finally, glushinskite tetrahedral crystals growing on chrysotile fibers were observed in the SEM images (Fig. 10c).

At pH 3–4, no mineralogical or compositional changes were observed by XRD, FTIR, or SEM analyses after dissolution. A general description is possible. Figure 5 shows the release of Si and Mg in a representative experiment at pH 4 with and without oxalate. The catalytic effect of oxalate is still clear from the beginning of the experiments at pH 3 and 4. The amount of Si and Mg dissolved is up to 6–7 times higher in the presence of oxalate at pH 4. Moreover, the Mg/Si concentration ratio increases from 1.6 to 3 because of the capacity of oxalate to form stable complexes with aqueous Mg at pH 3 to 9 (Fig. 9b). The formation of this aqueous complex does not occur at pH 2 because the oxalate species ($C_2O_4^{2-}$named as Ox^{2-} in figure 11c) is not available (Fig. 9c). Following the speciation diagrams, the availability of the species Mg^2 and $C_2O_4^{\tilde{2}}$ at pH 3–6 contributes to the increase in dissolution rates. Based on these results, two mechanisms can contribute to the catalysis of chrysotile dissolution rates in oxalate solutions:

1) The formation of aqueous magnesium oxalate complexes is favored at pH 3 to 6 by the predominance of $C_2O_4^{\tilde{2}}$ and Mg^{2+} species (Figs. 9b and 9c). The formation of this soluble complex shifts reaction (8) to the right, decreasing the IAP and ΔG_r values. However, the design of batch experiments per se does not allow observing a significant change in ΔG_r (Table 5).

2) The nucleophilic attack of $C_2O_4^{\tilde{2}}$ anions on the $>MgOH_2^+$ surface sites produce $>Mg–C_2O_4$ surface complexes and subsequent fast detachment of the complex from the surface. Oxalate anion is the reactive species, whose catalytic effect is favored at pH > 4.2 (pK_{a2} for oxalic acid). This is why at lower pH, where the dominant species are hydrogen oxalate and oxalic acid, other mechanisms are present, such as the precipitation of glushinskite at pH 2 or the complete dissolution of the brucite sheet at pH 1. These processes need to be studied in detail, as they may have a potential utility in remediation of chrysotile-contaminated sites.

Finally, at pH 7 and above, oxalate does not have any effect on the dissolution rates. Although the formation of the aqueous magnesium oxalate complex between pH 7 to approximately 9.5 is still favored, Mg^2 is not available because of its low solubility at these pH values.

IMPLICATIONS

Classic dissolution studies used in geochemistry provide easy and reliable data, which can be used as a valuable background for many other fields. In our case, the complete outline of dissolution rates versus pH in presence of inorganic and oxalate solutions can be useful to design and select optimal conditions during carbon capture processes. Most efficient processes suggested for carbonation involve leaching or dissolution of silicates in liquid media and precipitation of magnesium as carbonates or hydroxides for subsequent carbonation (Huijgen and Comans, 2003, 2005). However available data on mineral and organic acids treatments are scarce and occasionally contradicting. Our dataset quantifies dissolution in the complete scale of pH showing that chrysotile dissolves faster in acid media and oxalate acts as a strong catalyst increasing the efficiency of magnesium release to the solution at ambient temperature, which decreases the energetic cost of the process. Although in vitro experiments do not reproduce the complexity of processes that can occur in human body, they provide a benchmark to understand the degradation of inhaled particles. Kinetic experiments designed to evaluate chrysotile dissolution rates in solutions containing organic ligands as oxalate may contribute to the understanding of the solution/mineral interaction and to estimate the biodurability of chrysotile particles in lung-fluids.

ACKNOWLEDGMENTS

Financial support was obtained from Project P07-RNM-02772 (Junta de Andalucía); MR benefited from a JAE-Doc contract with CSIC with contribution from the FEDER funds (EU). The authors thank Carlos Jové Colón for helpful advice on including oxalate complexes in the LLNL database for EQ3NR, Laura Delgado for statistical analysis and Eduardo Flores for assistance with laboratory work. FJH, amdg

REFERENCES

Allen, M., Smith R. (1994) Dissolution of fibrous silicates in acid and buffered salt solutions. Minerals Engineering, 7, 1527–1537.

ATSDR (2001) Toxicological profile for asbestos. Agency for Toxic Substances and Disease Registry, Atlanta.

Anbalagan, G. Sivakumar, G., Prabakaran, A.R., Gunasekaran, S. (2010) Spectroscopic characterization of natural chrysotile. Vibrational Spectroscopy, 52, 122-127.

Bales, R.C., Morgan, J.J. (1985) Dissolution kinetics of chrysotile at pH 7 to10. Geochimica et Cosmochimica Acta, 49, 2281–2288.

Bergman, P.D., and Winter, E.M. (1995) Disposal of carbon dioxide in aquifers in the US. Energy Conversion and Management, 36, 523-526.

Bibi, I., Singh, B., Silvester, E. (2011) Dissolution of illite in saline-acidic solutions at 25ºC. Geochimica et Cosmochimica Acta, 75, 3237-3249.

Brantley, S. L. and Chen, Y., (1995) Chemical weathering rates of pyroxenes and amphiboles. In Chemical Weathering Rates of Silicate Minerals, Vol. 31 (ed. A. F. White and S. L. Brantley), pp. 119–172. Mineralogical Society of America.

Cama, J. and Ganor, J. (2006) The effects of organic acids on the dissolution of silicate minerals: A case study of oxalate catalysis of kaolinite dissolution. Geochimica et Cosmochimica Acta, 70, 2191-2209.

Choi, I. and Smith R.W. (1972) Kinetic study of dissolution of asbestos fibers in water. Journal of Colloid and Interface Science, 40, 253-262.

Favero-Longo, S.E., Turci, F., Tomatis, M., Castelli, D., Bonfante, P., Hochella, M.F., Piervittori, R., Fubini, B. (2005) Chrysotile asbestos is progressively converted into a

non-fibrous amorphous material by the chelating action of lichen metabolites. Journal of Environmental Monitoring, 8, 764-766.

Fernández, R., Cuevas, J., Sánchez, L., Vigil de la Villa, R., Leguey, S. (2006) Reactivity of the cement–bentonite interface with alkaline solutions using transport cells. Applied Geochemistry, 21, 977-992.

Franklin, S.P., Hajash, A.J., Dewers, T.A.,Tieh, T.T. (1994) The role of carboxylic acids in albite and quartz dissolution: an experimental study under diagenetic conditions. Geochimica et Cosmochimica Acta, 58, 4259-4279.

Grasshoff, K., Ehrhardt, M., Kremling, K. (1983) *Methods of Seawater Analysis*, 2nd ed. Verlag Chemie.

Gunter, M.E., Belluso, E., and Mottana, A. (2007a) Amphiboles: Environmental and health concerns. In Amphiboles: Crystal Chemistry, Occurrences, and Health Concerns, Reviews in Mineralogy and Geochemistry, 67, 453-516.

Gunter, M.E., Sanchez, M.S., and Williams, T.J. (2007b) Characterization of chrysotile samples for the presence of amphiboles from the Carey Canadian deposit, southeastern Quebec, Canada. Canadian Mineralogist, 45, 263-280.

Halder, S. and Walther, J.V. (2011) Far from equilibrium enstatite dissolution rates in alkaline solutions at earth surface conditions. Geochimica et Cosmochimica Acta, 75, 7486-7493.

Hargreaves, A. andTaylor, W.J. (1946) An X-ray examination of decomposition products of chrysotile (asbestos) and serpentine. Mineralogical Magazine, 27, 204-216.

Huang, W.H. and Kiang, WC. (1972) Laboratory dissolution of plagioclase feldspar in water and organic acids at room temperature. American Mineralogist, 57, 1849-1859.

549 Hume, L.A. and Rimstidt, J. D. (1992) The biodurability of chrysotile asbestos. American
550 Mineralogist, 77, 1125-1128.

551 Hydes, D.J. and Liss, P.S. (1976) Fluorimetric methods for the determination of low
552 concentrations of dissolved aluminium in natural waters. Analyst, 101, 922-931.

553 Jurinski, J. B. and Rimstidt, J. D. (2001) Biodurability of talc. American Mineralogist, 86,
554 392-399.

555 Kalinowski, B.E. and Schweda, P. (2007) Rates and nonstoichiometry of vermiculite
556 dissolution at 22 ºC. Geoderma, 142, 197-209.

557 Kohler, S.J., Bosbach, D., Oelkers, E.H. (2005) Do clay mineral dissolution rates reach steady
558 state? Geochimica et Cosmochimica Acta, 69, 1997-2006.

559 Laidler, K. J. (1987) Chemical Kinetics (3rd Ed.) Harper and Row, New York.

560 LaDou, J., Castleman, B., Frank, A., Gochfeld, M., Greenberg, M., Huff, J., Hoshi, T.K.,
561 Landrigan, P.J., Lemen, R., Myers, J., Soffritti, M., Soskolne, C.L:, Takahashi, K.,
562 Teitelbaum, D., Terracini, B., Watterson, A. (2010) The case for a global ban on
563 asbestos. Environmental Health Perpectives, 118, 897-901.

564 Lasaga, A.C. (1995) Fundamental approaches to describing mineral dissolution and
565 precipitation rates. In Reviews in Mineralogy Volume 31: Chemical Weathering Rates
566 of Silicate Minerals (eds. A. F. White and S. L. Brantley). Mineralogical Society of
567 America, Washington, D.C. pp. 23-86.

568 Lin, F.C. and Clemency, V. (1981) The dissolution kinetics of brucite, antigorite, talc, and
569 phlogopite at room temperature and pressure. American Mineralogist, 66, 801-806.

570 Liu, Y., Olsen, A.A., Rimstidt, J.D. (2006) Mechanism for the dissolution of olivine series
571 minerals in acidic conditions. American Mineralogist, 91, 455-458.

572 Luce, R.W., Bartlett, R.W., Parks, G.A. (1972) Dissolution kinetics of magnesium silicates.
573 Geochimica et Cosmochimica Acta, 36, 35-50.

574 Metz V., Raanan H, Pieper H., Bosbach D., Ganor J. (2005) Towards the establishment of a
575 reliable proxy for the reactive surface area of smectite. Geochimica et Cosmochimica
576 Acta, 69, 2581-2591.

577 Nagy, K.L. (1995) Dissolution and precipitation kinetics of sheet silicates. Reviews in
578 Mineralogy, 31, 173-233.

579 Nagy, B., Bates, T. F. (1952) Stability of Chrysotile asbestos. American Mineralogist, 37,
580 1055-1058.

581 O'Connor, W.K., Dahlin, D.C., Nilsen, D.N., Gerdemann, S.J., Rush, G.E., Penner, L.R.,
582 Walters, R.P., Turner, P.C. (2002) Continuing studies on direct aqueous mineral
583 carbonation for CO_2 sequestration. The Proceedings of the 27th International Technical
584 Conference on Coal Utilization & Fuel Systems, pp. 819–830.

585 Oelkers, E.H., Sergey V.G., Claire C., Pokrovsky O.S. and Schott J. (2009) The surface
586 chemistry of multi-oxide silicates. Geochimica et Cosmochimica Acta 73, 4617-4634.

587 Oelkers, E. H. and Schott, J. (2001) An experimental study of enstatite dissolution rates as a
588 function of pH, temperature, and aqueous Mg and Si concentration, and the mechanism
589 of pyroxene/pyroxenoid dissolution. Geochimica et Cosmochimica Acta, 65, 1219–
590 1231.

591 Olsen, A.A. and Rimstidt, J.D. (2008) Oxalate-promoted forsterite dissolution at low pH.
592 Geochimica et Cosmochimica Acta, 72, 1758-1766.

593 Oze, C. and Solt, K. (2010) Biodurability of chrysotile and tremolite asbestos in simulated
594 lung and gastric fluids. American Mineralogist, 95, 825-831.

595 Park, A.-H., Jadhav, R., Fan, L.-S. (2003) CO_2 Mineral sequestration: chemically enhanced
596 aqueous carbonation of serpentine. Canadian Journal of Chemical Engineering 81 (3–4),
597 885–890.

598 Park, A.-H. and Fan, L.-S. (2004) CO_2 Mineral sequestration: physically activated dissolution
599 of serpentine and pH swing process. Chemical Engineering Science 59, 5241-5247.

600 Prigiobbe, V. and Mazzotti, M. (2011) Dissolution of olivine in the presence of oxalate,
601 citrate, and CO2 at 90°C and 120°C.Chemical Engineering Science, 66, 6544-6554.

602 Ramos, M.E., Cappelli, C., Rozalen, M., Fiore, S., Huertas, F.J. (2011) Effect of lactate,
603 glycine, and citrate on the kinetics of montmorillonite dissolution. American
604 Mineralogist, 96, 768-780.

605 Rimstidt, J. and Newcomb, W. (1993) Measurement and analysis of rate data: the rate of
606 reaction of ferric iron with pyrite. Geochim. Cosmochim. Acta, 57, 1919–1934.

607 Roggli, V.L. and Coin, P. (2004) Mineralogy of asbestos. In V.L. Roggli, T.D. Oury, and
608 T.A. Sporn, Eds., Pathology of Asbestos-Associated Diseases, 2nd edition, p. 1-16.
609 Springer, New York.

610 Rozalen, M. and Huertas, F.J. (2013) Comparative effect of chrysotile leaching in nitric,
611 sulfuric and oxalic acid at room temperature. Chemical Geology, 352, 134-142.

612 Rozalen, M.L., Huertas, F.J., Brady, P.V., Cama, J., Garcia-Palma, S., Linares, J. (2008)
613 Experimental study of the effect of pH on the kinetics of montmorillonite dissolution at
614 25°C. Geochimica Cosmochimica Acta, 72, 4224-4253.

615 Sillen, L.G. and Martell, A.E. (1964) Stability constants of metal-ion complexes. The
616 Chemical Society, London.

617 Skinner, H.C.W., Ross, M., Frondel, C. (1988) Asbestos and other fibrous materials, 222p.
618 Oxford University Press, U.K.

619 Sontevska, V., Jovanovski, G., Makreskin, P. (2007) Minerals from Macedonia. Part XIX.
620 Vibrational spectroscopy as identificational tool for some sheet silicate minerals.
621 Journal of Molecular Structure, 318–327.

622 Taunton, A.E., Druschel, G.K., Gunter, M.E., and Wood, S.A. (2010) Geochemistry in the
623 lung: Reaction-path modeling and experimental examinations of rock-forming minerals
624 under physiologic conditions. American Mineralogist, 95, 1624-1635.

625 Thomassin, J.H., Goni, J., Baillif, P., Touray, J.C., Jaurand, M.C. (1977) An XPS study of the
626 dissolution kinetics of chrysotile in 0. I N oxalic acid at different temperatures Physics
627 and Chemistry of Minerals, l, 385-398.

628 Turci, F., Tomatis, M., Mantegna, S., Cravotto, G. Fubini, B. (2008) A new approach to the
629 decontamination of asbestos-polluted waters by treatment with association of oxalic
630 acid and power ultrasound. Ultrasonics – Sonochemistry, 15, 420-427.

631 Turci, F., Colonna, M., Tomatis, M., Mantegna, S., Cravotto, G., Fubini, B. (2010) New
632 detoxification processes for asbestos fibers in the environment. Journal of Toxicology
633 and Environmental Health, 73, 368-377.

634 Van Gosen, B.S. (2007) The geology of asbestos in the United States and its practical
635 applications. Environmental and Engineering Geoscience, 13, 55–68.

636 Vieillard Ph. (2000) A new method for the prediction of Gibbs free energies of formation of
637 hydrated clay minerals based on the electronegativity scale. *Clays Clay Minerals* **48,**
638 459–473.

639 Virta, R.L. (2005) Mineral commodity profiles-asbestos. U.S. Geological Survey Circular
640 1255-KK.

641 Wang, X., Li, W., Hu, H., Zhang, T., Zhou, Y. (2005): Dissolution of kaolinite induced by
642 citric, oxalic, and malic acids. Journal of Colloid and Interface Science, 290, 481-488.

643 Wang, L., Lu, A., Wang, C., Zheng, X., Zhao, D., (2006) Nano-fibriform production of silica
644 from natural chrysotile. Journal of Colloid and Interface Science, 295, 436-439.

645 Wolery, T.J. (1992): EQ3NR, a computer program for geochemical aqueous speciation-
646 solubility calculations: theoretical manual, user's guide and related documentation
647 (version 7). UCRL-MA-110662 PT III. Laurence Livermore National Laboratory.

648 Wood, S.A., Taunton, A.E., Normand, C., and Gunter, M.E. (2006) Mineral-fluid interaction
649 in the lungs: Insights from reaction-path modeling. Inhalation Toxicology, 18, 975-
650 984.

651 Wypych, F., Adad, L.B., Mattoso, N., Marangon, A.A., Schreiner, W.H. (2005) Synthesis and
652 characterization of disordered layered silica obtained by selective leaching of octahedral
653 sheets from chrysotile and phlogopite structures. Journal ofColloid and Interface
654 Science, 283, 107-112.

655 Zysset, M. and Schindler, P.W. (1996) The proton promoted dissolution kinetics K-
656 montmorillonite. Geochimica et Cosmochimica Acta, 60, 921-931.

657

658 **FIGURE CAPTIONS**

659

660 Figure 1. Photograph of chrysotile veins growing into the fracture walls in Ojen outcrop.

661 Figure 2. SEM image of the morphology of the chrysotile fibers used as starting material.

662 Figure 3. Evolution of pH, Si, Mg concentration and Mg/Si atomic ratio along time for some
663 representative experiments at pH 3, 6 and 10. Horizontal lines in d, e and f represent
664 the stoichiometric ratio in the solid sample.

665 Figure 4. Evolution of pH, Si and Mg concentrations and Mg/Si atomic ratio along time for
666 some representative experiments with oxalate at pH 1, 2, 3 and 8. Horizontal lines in
667 b, d, f and h represent the stoichiometric ratio in the solid sample.

668 Figure 5. Si and Mg released in a representative experiment at pH 4 with and without oxalate.

669 Figure 6. Dissolution rates calculated from Si and Mg concentration data for the inorganic
670 buffered series CrLx versus pH.

671 Figure 7. XRD of a) initial chrysotile; b) chrysotile batch at pH 1 after 70 days of reaction; c)
672 chrysotile batch at pH 1 with oxalic buffer after 30 days of reaction.

673 Figure 8. SEM image of chrysotile dissolved at pH 1 with inorganic buffer (after 70 days of
674 reaction).

675 Figure 9. a) Re-calculated ”initial dissolution rates” derivated from Si concentration data for
676 the inorganic buffered (CrLx) series and oxalate series (CrOx) versus pH. b)
677 Magnesium (15mmol L^{-1}) speciation in solutions with 1 mmol L^{-1} of oxalate as a
678 function of the solution pH. c) Oxalic acid speciation as a function of solution pH.

679 Figure 10. Solid sample after treatment at pH 2 (a) XRD (b) FTIR (c) SEM

TABLES

Table 1. Composition of the initial solutions used as buffers in the dissolution experiments.

Initial pH	HNO_3 (mol L^{-1})	CH_3COOH (mol L^{-1})	KCH_3COO (mol L^{-1})	$KHCO_3$ (mol L^{-1})	K_2CO_3 (mol L^{-1})	KOH (mol L^{-1})	KNO_3 (mol L^{-1})	Na-Ox (mol L^{-1})
Series CrLx								
1.06	0.1	-	-	-	-	-	0.01	-
1.89	0.01	-	-	-	-	-	0.01	-
3.13	0.001	-	-	-	-	-	0.01	-
4.08	-	0.0085	0.0015	-	-	-	0.01	-
5.28		0.0035	0.0064				0.01	-
6.52		0.0009	0.009				0.01	-
8.32				0.0021			0.01	-
9.59				0.0095	0.0005		0.01	-
10.57				0.1	0.1		0.01	-
11.89						0.005	0.01	-
12.85						0.05		-
13.78						0.5		-
								-

Initial pH	HNO_3 (mol L^{-1})	CH_3COOH (mol L^{-1})	KCH_3COO (mol L^{-1})	$KHCO_3$ (mol L^{-1})	K_2CO_3 (mol L^{-1})	KOH (mol L^{-1})	KNO_3 (mol L^{-1})	Na-Ox mol L^{-1}
Series CrOx *								
1.21	0.1						0.01	0.015
2.19	0.01						0.01	0.015
3.18	0.001						0.01	0.015
4.16	-	0.0085	0.0015	-	-	-	0.01	0.015
5.18	-	0.0035	0.0064				0.01	0.015
5.78	-	0.0009	0.009				0.01	0.015
6.22	-	-	-	0.00025	-	-	0.01	0.015
8.28	-	-	-	0.0021	-	-	0.01	0.015
8.90	-	-	-	0.0095	0.0005	-	0.01	0.015
9.89	-	-	-	0.1	0.1	-	0.01	0.015
11.58	-	-	-	-	-	0.005	0.01	0.015
12.44	-	-	-	-	-	0.05	0.01	0.015
13.30	-	-	-	-	-	0.5	0.01	0.015

* All the experiments with oxalate also have 2 ppm of NaN_3 added as a bactericide

Table 2. Stability constants for oxalic acid (H_2Ox) and aqueous Mg^{2+}-oxalate complexes.

Reaction	Constant	Reference
$H_2Ox = HOx^- + H^+$	$pK_1 = 1.27$	(a)
$HOx^- = Ox^{2-} + H^+$	$pK_2 = 4.26$	(a)
$Mg^{2+} + Ox^{2-} = Mg(Ox)_{aq}$	$\log K_1 = 2.10$	(b)
$Mg^{2+} + 2Ox^{2-} = Mg(Ox)_2^{2-}$	$\log\beta_2 = 6.67$	(b)

[a]EQ3/6 database (Wolery, 1992), [b]Sillen and Martell (1964).

Table 3. Experimental conditions and results of the dissolution experiments in batch reactors for series CrLx_1m (1 month and 2 g L^{-1}) and CrLx_15d (15 days and 0.1 g L^{-1}). ΔG_r values correspond with the biggest and smaller values obtained form EQ3NR calculations for every experiment. Shadowed values correspond to saturation conditions.

Batch	pH in	pH out average	log R Si (mol $m^{-2}s^{-1}$)	log R Mg (mol $m^{-2}s^{-1}$)	ΔG_r (kcal mol^{-1})	
CrLx_1m_1	1.06	1.25	-11.16	-10.44	-58.56	-47.45
CrLx_1m_2	1.89	2.41	-11.47	-11.12	-50.31	-36.54
CrLx_1m_3	3.13	4.00	-12.06	-11.00	-41.89	-31.23
CrLx_1m_4	4.08	4.10	-12.10	-12.05	-36.69	-31.55
CrLx_1m_5	5.28	7.53	-12.91	-13.51	-28.24	-7.55
CrLx_1m_6	6.52	7.61	-12.91	-13.31	-17.16	-8.69
CrLx_1m_8	8.32	8.33	-12.93	-13.71	-5.22	-3.79
CrLx_1m_9	9.59	9.41	-12.88	-14.78	1.28	1.45
CrLx_1m_10	10.57	10.40	-12.74	-	0.59	-0.03
CrLx_1m_11	11.83	11.57	-12.68	-	8.08	10.64
CrLx_1m_12	12.85	12.68	-12.66	-	4.24	7.04
CrLx_1m_13	13.78	13.61	-12.58	-	-0.96	7.01
CrLx_15d_10	10.36	10.35	-12.22	-	-5.82	-4.35
CrLx_15d_11	11.68	11.67	-12.19	-	5.39	6.49
CrLx_15d_12	12.64	12.62	-12.24	-	2.47	3.32
CrLx_15d_13	13.55	13.54	-12.16	-	-0.57	-0.15

Table 4. Saturation state (kcal·mol^{-1}) of the initial and final output solutions (1 to 30 days) computed for the CrLx series according to Eq. (3). Shadowed values correspond to saturation conditions.

Serie	pH out	Ctl		Qtz		SiO_2(am)		Brc		Mgs	
CrLx_1m_1	1.25	-58.60	-47.48	0.21	1.83	-1.54	0.08	-24.12	-21.49	-20.44	-17.82
CrLx_1m_2	2.41	-52.62	-36.56	-0.02	1.51	-1.77	-0.24	-21.97	-17.64	-18.30	-13.97
CrLx_1m_3	4.00	-41.91	-31.24	-0.11	0.93	-1.86	-0.83	-18.34	-15.47	-14.67	-11.80
CrLx_1m_4	4.10	-36.30	-31.57	0.07	0.82	-1.68	-0.69	-16.59	-15.51	-12.92	-11.84
CrLx_1m_5	7.53	-28.26	-7.56	-0.39	0.18	-2.14	-1.57	-13.60	-7.08	-9.93	-3.41
CrLx_1m_6	7.61	-17.17	-8.70	-0.27	0.15	-2.02	-1.60	-9.98	-7.45	-6.32	-3.77
CrLx_1m_8	8.33	-5.23	-3.80	-3.31	0.13	-2.06	-1.62	-5.98	-5.80	-2.31	-2.13
CrLx_1m_9	9.41	-1.27	-1.45	-0.24	0.23	-1.99	-1.53	-3.86	-4.11	-0.19	-0.44
CrLx_1m_10	10.40	-1.05	-0.06	-0.85	-0.20	-2.60	-1.96	-4.34	-4.33	-0.34	-0.65
CrLx_1m_11	11.57	8.08	10.64	-2.63	-1.34	-4.37	-3.09	EQ	EQ	-	-
CrLx_1m_12	12.68	4.23	7.04	-4.55	-3.15	-6.30	-4.90	EQ	EQ	-	-
CrLx_1m_13	13.61	-1.02	6.98	-7.17	-3.17	-8.93	-4.93	EQ	EQ	-	-
CrLx_15d_10	10.35	-5.89	-4.41	-	-	-	-	-4.98	-4.72	-1.30	-1.04
CrLx_15d_11	11.67	5.39	6.50	-	-	-5.72	-5.17	EQ	EQ	-	-
CrLx_15d_12	12.62	2.47	3.31	-	-	-7.19	-6.76	EQ	EQ	-	-
CrLx_15d_13	13.54	-0.57	-0.16	-	-	-8.71	-8.50	EQ	EQ	-	-

*Ctl: chrysotile; Qtz: quartz; SiO_2(am): amorphous silica; Brc: brucite; Mgs: magnesite; EQ.: mineral/solution equilibrium.

Table 5. Comparison of the "initial rates" calculated for the dissolution experiments (only for comparison purposes) in batch reactors for series CrLx (inorganic buffers) and CrOx (15 mmol L^{-1} oxalate). Shadowed values correspond to saturation conditions

Batch	pH_{out}	Initial log R Si (mol $m^{-2}s^{-1}$)	Initial log R Mg (mol $m^{-2}s^{-1}$)	ΔG_r (kcal mol^{-1}) 6 days	Batch	pH_{out}	Initial log R Si (mol $m^{-2}s^{-1}$)	Initial log R Mg (mol $m^{-2}s^{-1}$)	ΔG_r (kcal mol^{-1}) 6 days
CrLx_1m_1	1.05	-11.59	-10.48	-56.92	CrOx_1m_1	1.18	-11.33	-10.33	-52.72
CrLx_1m_2	1.98	-11.67	-11.30	-50.29	CrOx_1m_2	2.55	-11.23	-	-39.65
CrLx_1m_3	3.40	-11.76	-11.63	-37.60	CrOx_1m_3	3.35	-11.09	-10.91	-35.76
CrLx_1m_4	4.07	-11.88	-11.83	-36.28	CrOx_1m_4	4.13	-11.10	-10.92	-31.47
CrLx_1m_5	5.68	-12.01	-12.23	-19.76	CrOx_1m_5	5.44	-11.14	-11.67	-22.54
CrLx_1m_6	6.80	-12.02	-12.44	-14.73	CrOx_1m_6	6.03	-11.51	-12.25	-18.33
	-	-	-	-	CrOx_1m_7	6.94	-12.14	-	-16.37
CrLx_1m_8	8.31	-12.02	-12.50	-4.48	CrOx_1m_8	8.39	-12.22	-12.69	-6.93
CrLx_1m_9	9.54	-11.83	-	1.47	CrOx_1m_9	8.93	-12.20	-14.22	-3.93
CrLx_15d_10	10.37	-11.81	-	-0.16	CrOx_1m_10	9.94	-11.87	-	1.31
CrLx_15d_11	11.72	-11.66	-	9.82	CrOx_1m_11	11.54	-11.60	-	9.23
CrLx_15d_12	12.67	-11.63	-	6.32	CrOx_1m_12	12.53	-11.49	-	6.54
CrLx_15d_13	13.59	-11.41	-	6.11	CrOx_1m_13	13.40	-11.34	-	6.85

Table 6. Saturation state (kcal·mol^{-1}) of the output solutions after 6 days computed for the CrOx series according to Eq. (3). Shadowed values correspond to saturation conditions.

Serie	pH out	Ctl	Qtz	SiO_2(am)	Brc	Mgs
CrOx_1m_1	1.18	-52.75	0.74	-1.01	-22.52	-16.52
CrOx_1m_2	2.55	-39.67	0.79	-0.96	-18.19	-14.52
CrOx_1m_3	3.35	-35.78	0.99	-0.76	-17.03	-13.36
CrOx_1m_4	4.13	-31.49	1.01	-0.74	-15.61	-11.94
CrOx_1m_5	5.44	-22.49	1.04	-0.71	-12.63	-8.96
CrOx_1m_6	6.03	-18.33	0.50	-1.24	-10.89	-7.22
CrOx_1m_7	6.94	-16.38	-0.14	-1.89	-9.81	-6.14
CrOx_1m_9	8.39	-6.93	-0.25	-2.00	-6.59	-2.92
CrOx_1m_10	8.93	-3.94	-0.36	-2.11	-5.52	-1.84
CrOx_1m_11	9.94	1.30	-0.45	-2.20	-3.71	-0.04
CrOx_1m_12	11.54	9.23	-2.05	-3.80	EQ	-
CrOx_1m_13	12.53	6.83	-3.39	-5.15	EQ	-
CrOx_1m_14	13.40	6.83	-3.25	-5.00	EQ	-

*Ctl: chrysotile; Qtz: quartz; SiO_2(am): amorphous silica; Brc: brucite; Mgs: magnesite; EQ.: mineral/solution equilibrium

Table 7 Band assignments in the FTIR spectrum of chrysotile and glushinskite

[a]Chrysotile cm^{-1}	Assignments	[b]Glushinskite	Assignments
3690 s	ν(OH) [a]	1664 vs	antisymmetric stretching oxalate group
3645 w	ν(OH) [a]	1641 vs	
1086 s	ν(Si-OH-Si) [b]	1373 m	symmetric stretching oxalate group
1020 sh	ν(Si-OH-Mg) [b]	1326 vs	
962 vs	ν(Si-OH-Si) [a]	830 m	
604 s	δ(OH) [a]	693 m	
558 s	Out-of-plane bending mode of Si-O [a]	500 s	
434 vs	δ(Si-O-Si) [b]	422 s	

s, strong; m, medium; w, weak; sh, shoulder; v, very.

[a] Anbalagan et al. (2010)

[b] Sontevska et al. (2007)

Figure 1

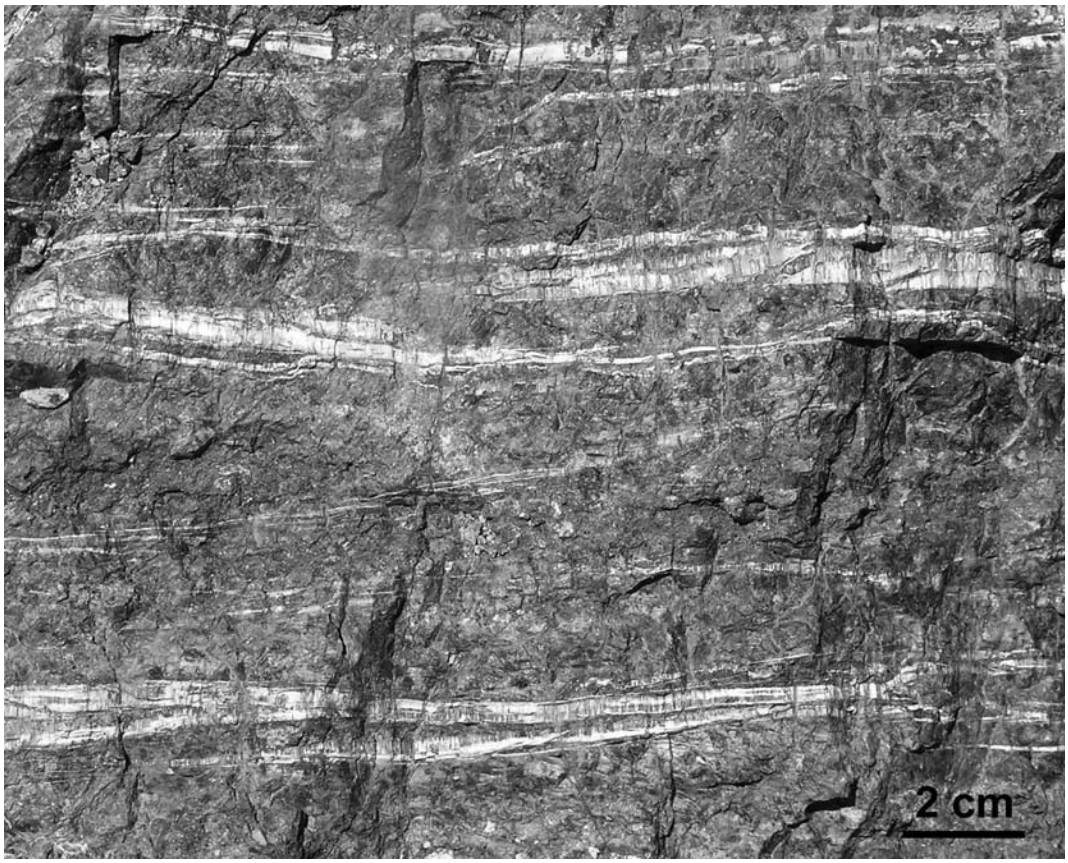

Figure 2

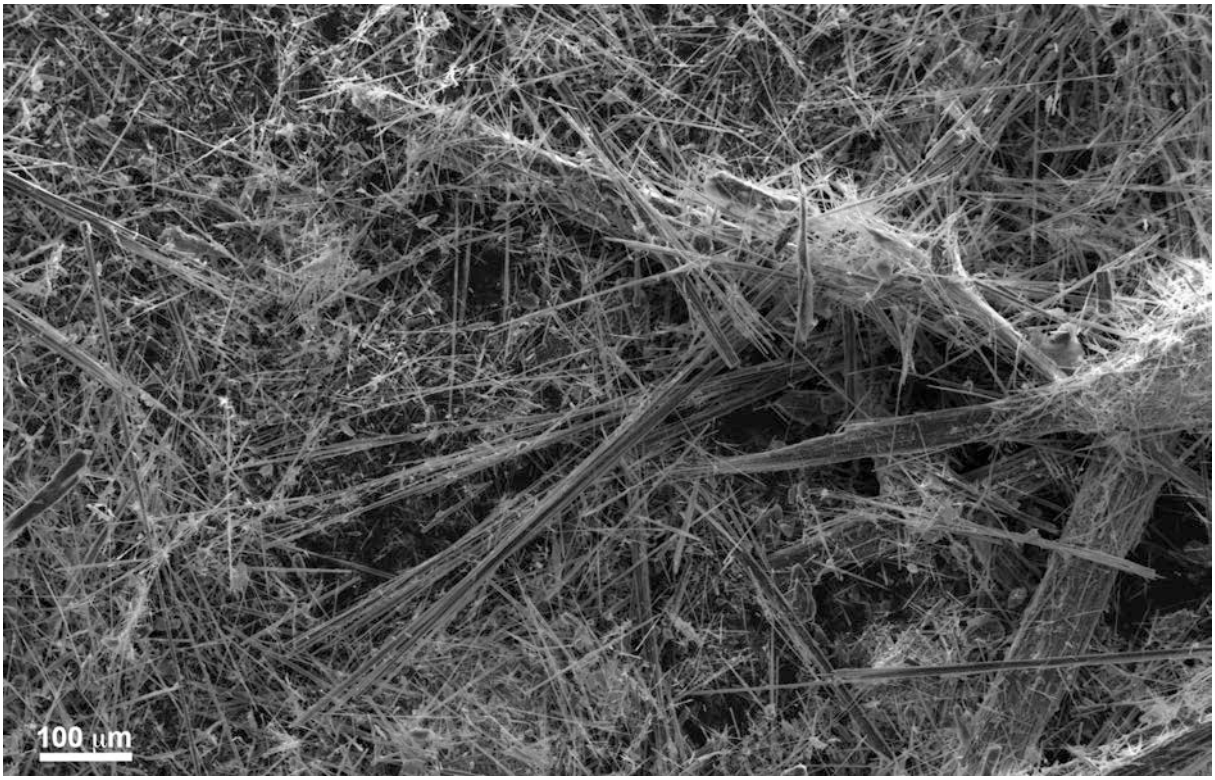

Figure 3

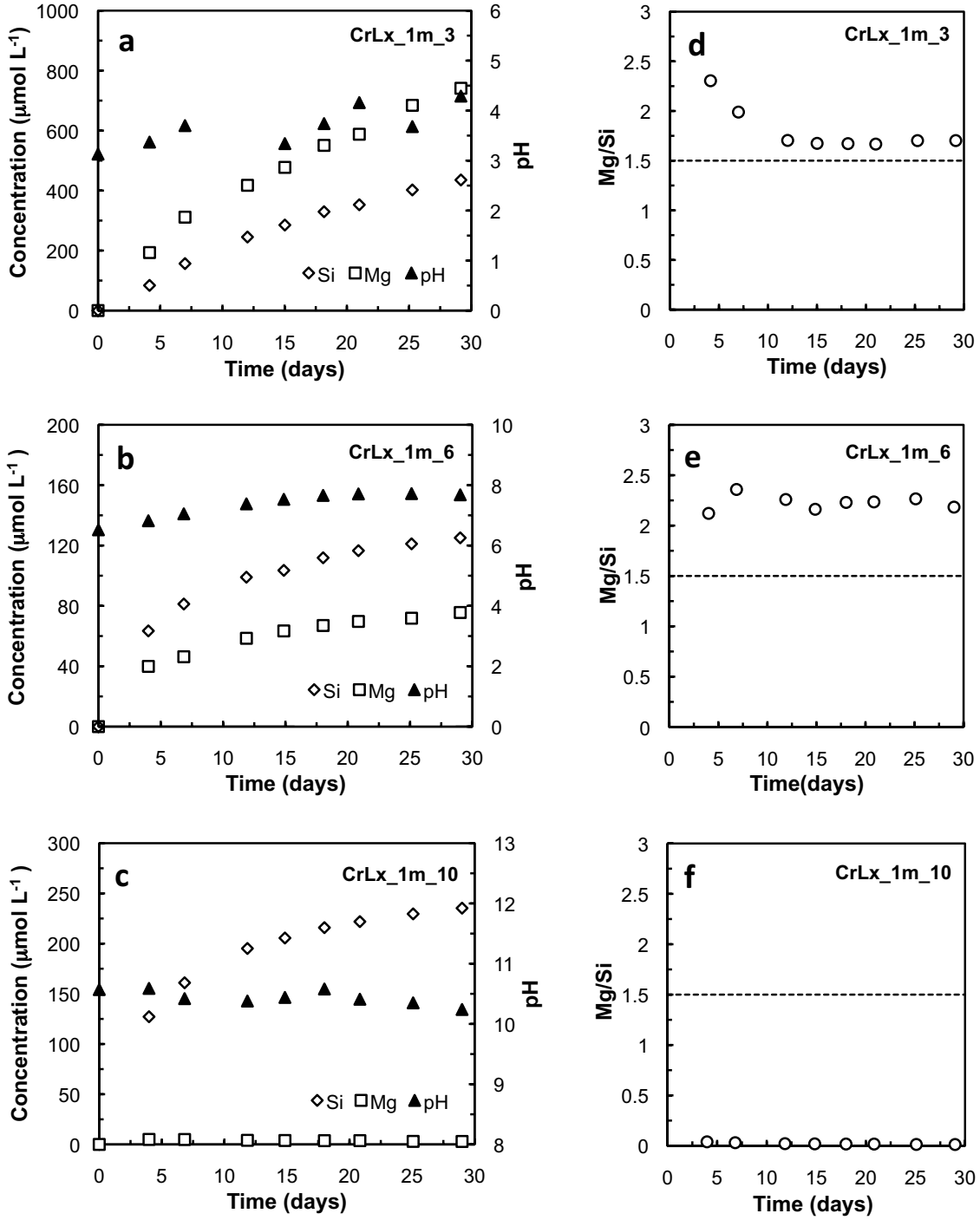
a
CrLx_1m_3
Concentration (µmol L-1)
pH
Si Mg pH
Time (days)
d
CrLx_1m_3
Mg/Si
Time (days)
b
CrLx_1m_6
Concentration (µmol L-1)
pH
Si Mg pH
Time (days)
e
CrLx_1m_6
Mg/Si
Time(days)
c
CrLx_1m_10
Concentration (µmol L-1)
pH
Si Mg pH
Time (days)
f
CrLx_1m_10
Mg/Si
Time (days)

Figure 4

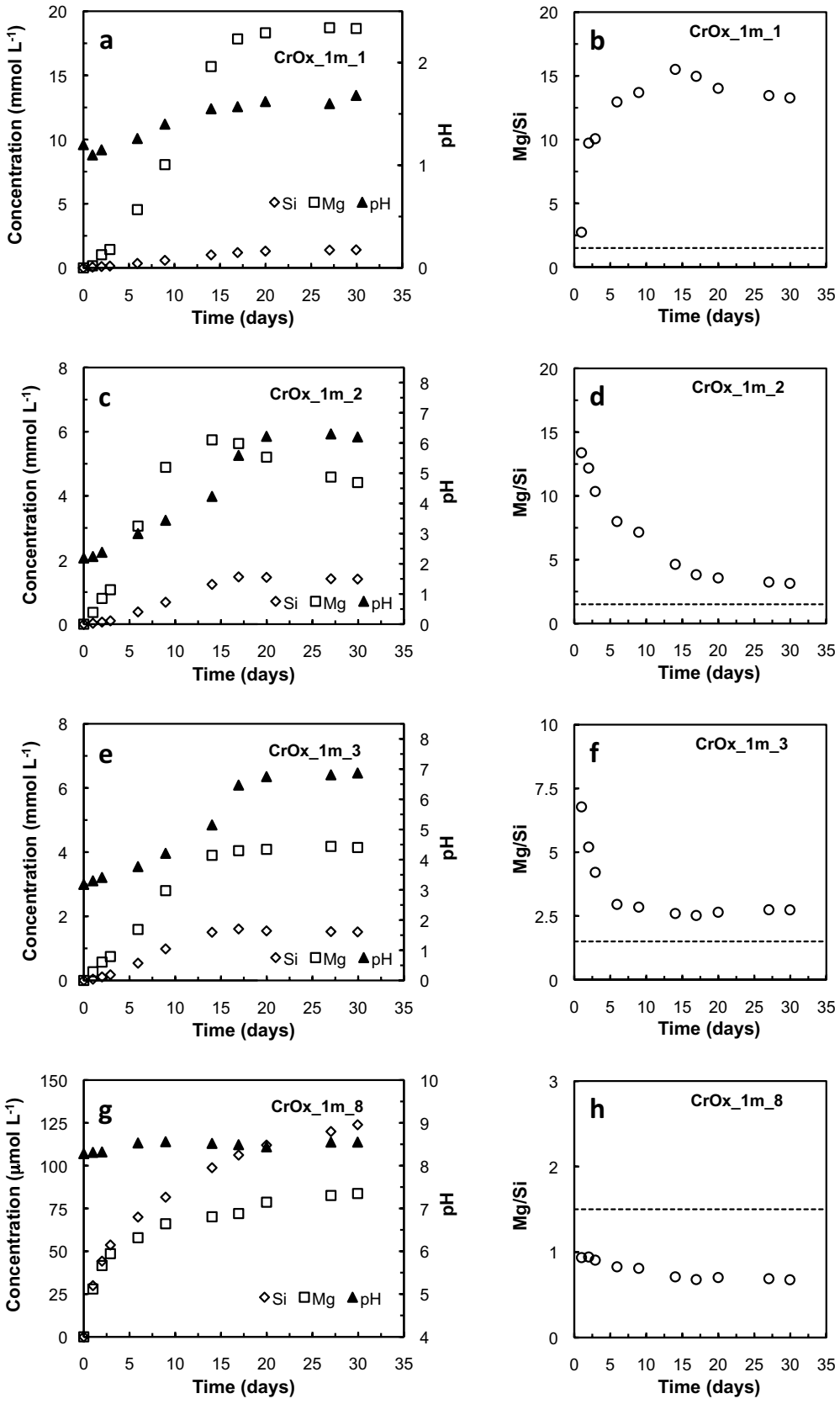
a
CrOx_1m_1
Concentration (mmol L-1)
pH
Si Mg pH
Time (days)
b
CrOx_1m_1
Mg/Si
Time (days)
c
CrOx_1m_2
Concentration (mmol L-1)
pH
Si Mg pH
Time (days)
d
CrOx_1m_2
Mg/Si
Time (days)
e
CrOx_1m_3
Concentration (mmol L-1)
pH
Si Mg pH
Time (days)
f
CrOx_1m_3
Mg/Si
Time (days)
g
CrOx_1m_8
Concentration (µmol L-1)
pH
Si Mg pH
Time (days)
h
CrOx_1m_8
Mg/Si
Time (days)

Figure 5

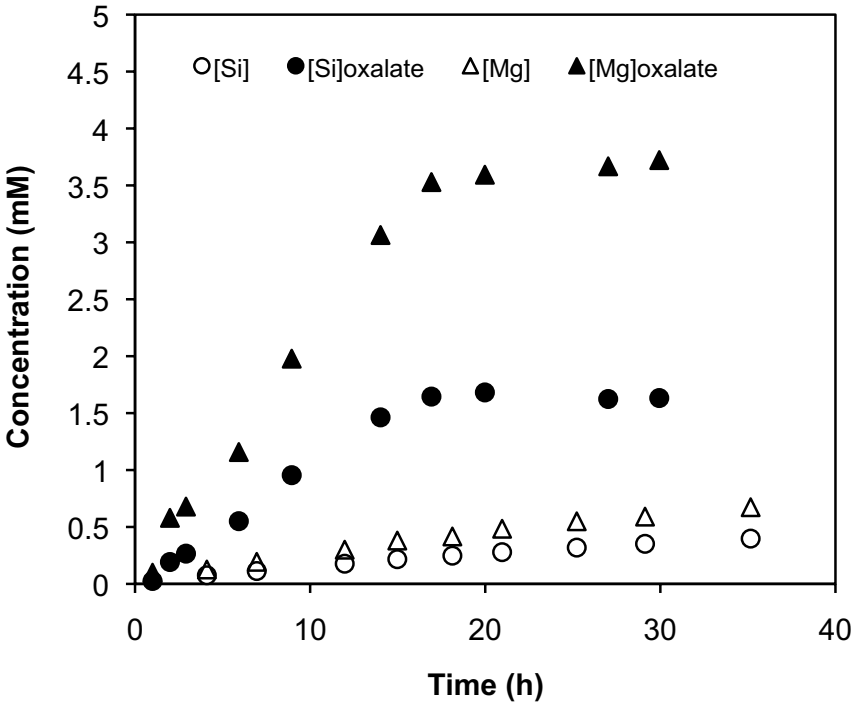
[Si]
[Si]oxalate
[Mg]
[Mg]oxalate
Concentration (mM)
Time (h)
0
0.5
1
1.5
2
2.5
3
3.5
4
4.5
5
0
10
20
30
40

Figure 6

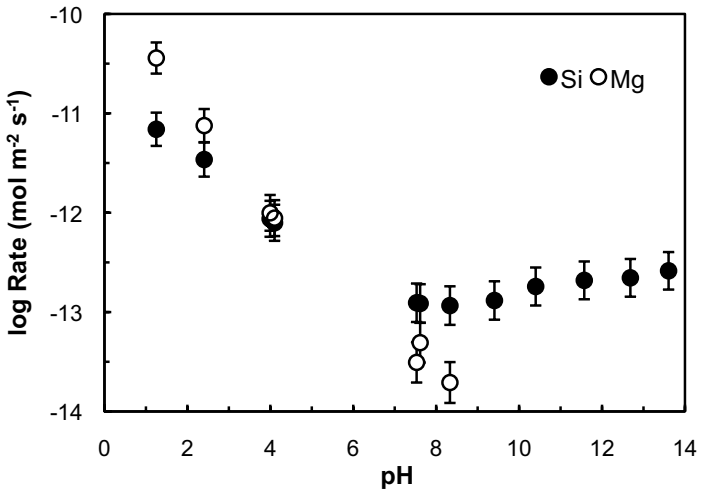

Figure 7

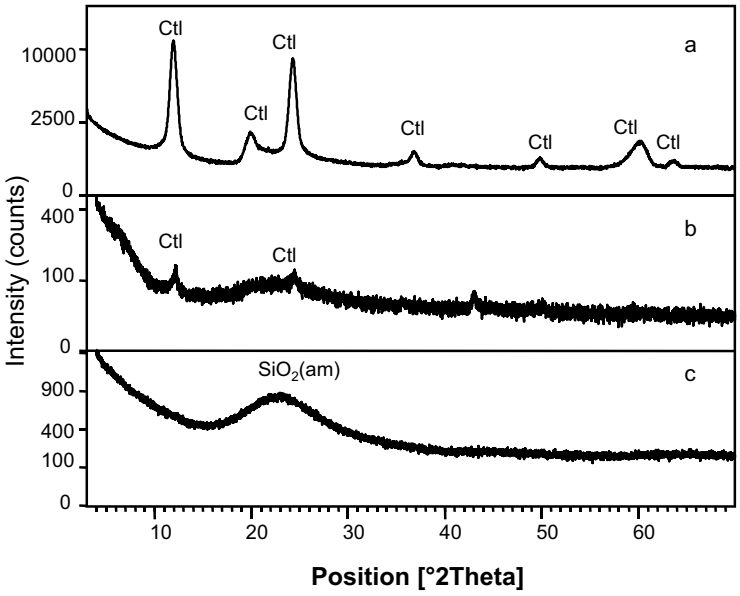
Ctl
Ctl
Ctl
Ctl
Ctl
Ctl
Ctl
a
10000
2500
0
Ctl
Ctl
b
400
100
0
SiO2(am)
c
900
400
100
0
Intensity (counts)
10
20
30
40
50
60
Position [°2Theta]

Figure 8

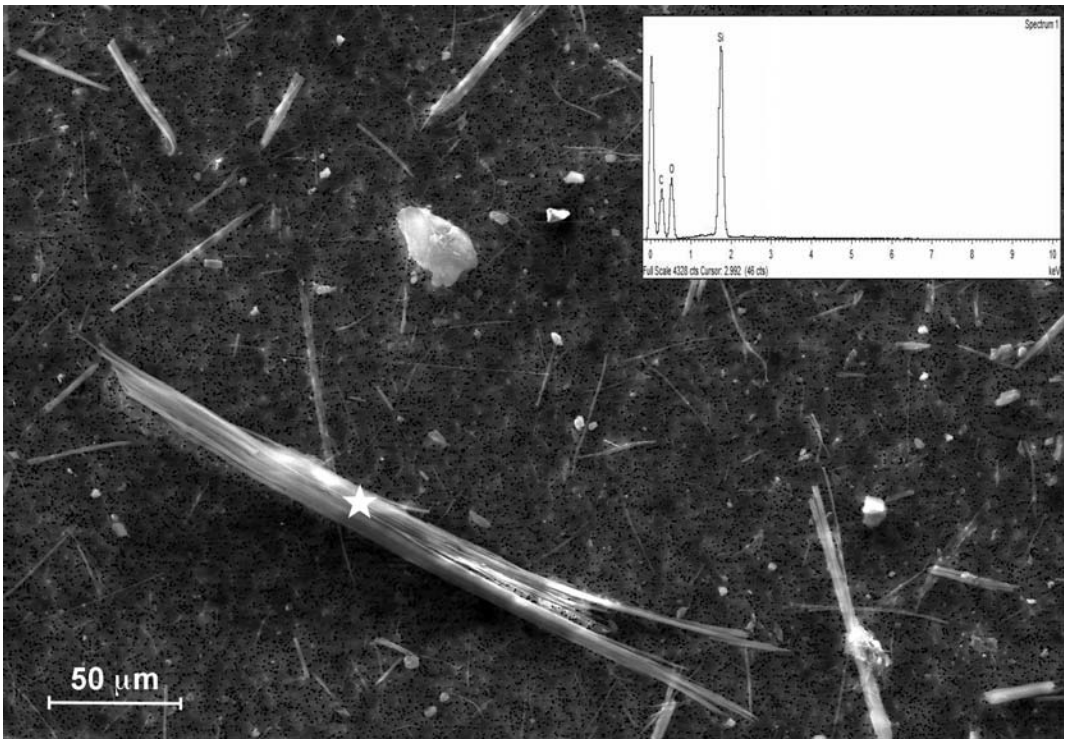
Spectrum 1
Si
C
O
0
1
2
3
4
5
6
7
8
9
10
Full Scale 4328 cts Cursor: 2.992 (46 cts)
keV
50 µm

Figure 9

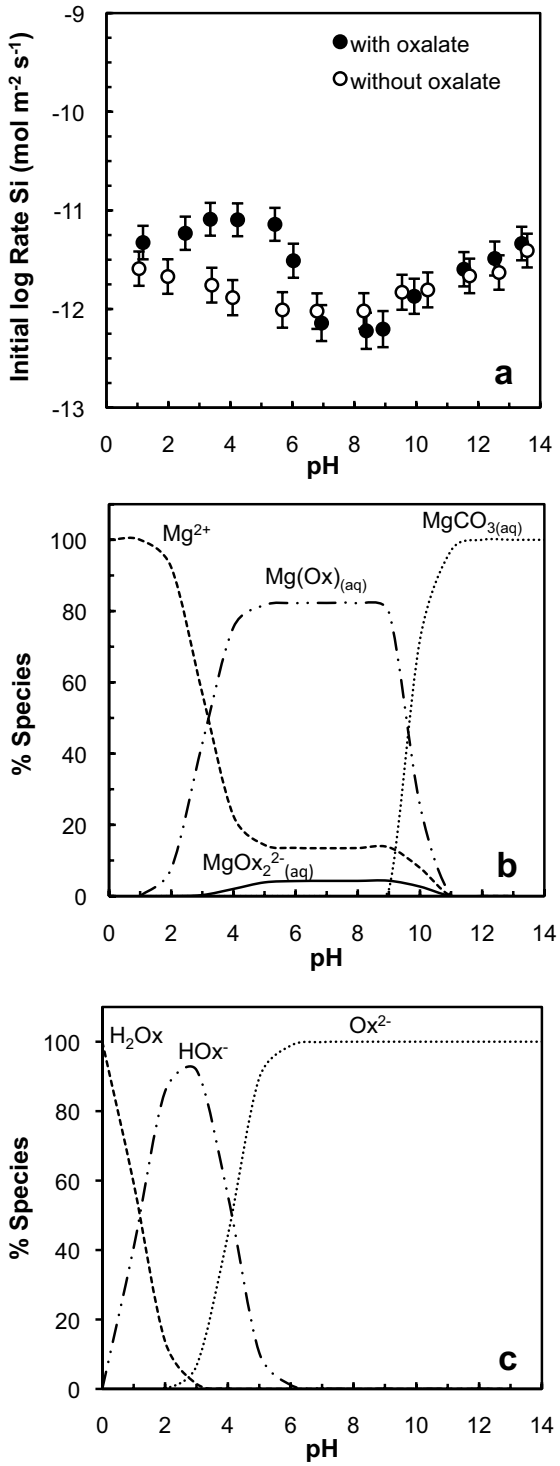
Initial log Rate Si (mol m-2 s-1)
-9
-10
-11
-12
-13
with oxalate
without oxalate
a
0
2
4
6
8
10
12
14
pH
% Species
100
80
60
40
20
0
Mg2+
Mg(Ox)(aq)
MgCO3(aq)
MgOx2 2-(aq)
b
pH
H2Ox
HOx-
Ox2-
c

Figure 10

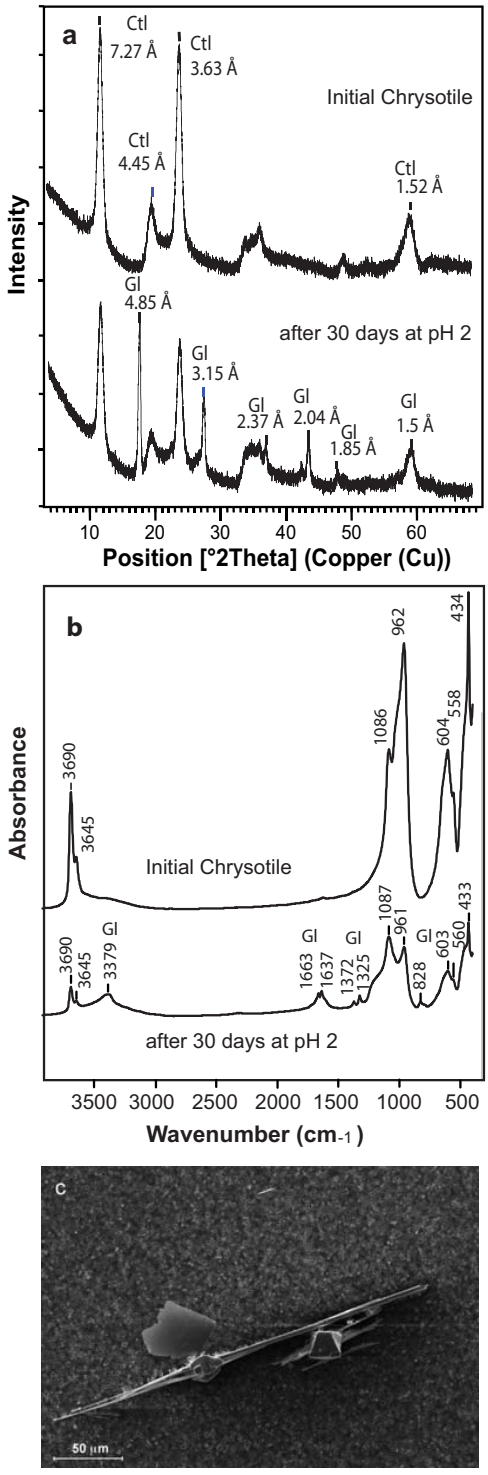
a
Ctl
7.27 Å
Ctl
3.63 Å
Initial Chrysotile
Ctl
4.45 Å
Ctl
1.52 Å
Intensity
Gl
4.85 Å
after 30 days at pH 2
Gl
3.15 Å
Gl
2.37 Å
Gl
2.04 Å
Gl
1.85 Å
Gl
1.5 Å
10 20 30 40 50 60
Position [°2Theta] (Copper (Cu))
b
962
434
1086
604
558
3690
3645
Absorbance
Initial Chrysotile
1087
961
433
Gl
Gl
Gl
Gl
3690
3645
3379
1663
1637
1372
1325
828
603
560
after 30 days at pH 2
3500 3000 2500 2000 1500 1000 500
Wavenumber (cm-1)
c
50 µm